Antenna sub-array switching strategy for low-cost & high-resolution radio-astronomical imaging

Jianhua Wang*, Lucien Bacharach*, Mohammed Nabil El Korso‡, Pascal Larzabal*
* *SATIE,* ‡ *L2S, Université Paris-Saclay, 91190 Gif-sur-Yvette, France*

2023 IEEE International Conference on Signal Processing, Communications and Computing (ICSPCC) | 979-8-3503-1672-8/23/$31.00 ©2023 IEEE | DOI: 10.1109/ICSPCC59353.2023.10400346

***Abstract*—This paper addresses the problem of optimizing imaging quality in radio-astronomy through antenna sub-arrays exploitation. A strategy for switching antenna sub-arrays is proposed to improve imaging quality and reduce computational complexity thanks to the drastic reduction of simultaneously used visibilities. The imaging algorithm is formulated based on the expectation-maximization (EM) algorithm, leveraging the correlation between antenna sub-arrays. Numerical simulations are conducted using sub-arrays designed by the Cramér-Rao bound (CRB) and the Barankin Bound (BRB) criteria to validate the proposed strategy. The imaging quality is evaluated using the normalized mean square error (NMSE) and structural similarity (SSIM) metrics, both globally and locally. Results demonstrate that the proposed antenna sub-array switching strategy effectively enhances imaging quality while reducing computational complexity.**

***Index Terms*—Antenna array processing, radio inteferometry, radio-astronomy imaging, EM algorithm.**

I. Introduction

Radio-astronomy telescope technology has made significant progress in the last decades, with the number of antennas increasing from tens to thousands and even millions. For instance, the SKA (Square Kilometer Array) project [1–3] involves over a hundred thousand antennas. However, processing data from all these antennas presents a formidable challenge due to limitations in data transmission, the big need for high precision analog-to-digital converters, and high computational complexity. Therefore, efficient techniques for exploiting antenna arrays are crucial to overcome these challenges.

By carefully selecting a subset of antennas, it is possible to significantly reduce the computational load without excessively sacrificing imaging quality. Antenna selection has been widely studied in the literature, with conventional techniques primarily focusing on optimizing the U-V coverage of the antenna array [4]. However, these methods are not necessarily optimal in terms of statistical performance. As a result, various antennas selection techniques based on estimation lower bounds have been proposed, including the Cramér-Rao bound (CRB) [5–7] and the Barankin bound (BRB) [8]. These techniques leverage the statistical performance of the radio-astronomical imaging estimators. Among them, the CRB-based antennas selection method offers advantages in terms of a closed-form expression and asymptotic performance, while the BRB-based method provides greater accuracy for finite sample sizes, considering the effect of ambiguity in small-sized samples or low signal-to-noise ratio (SNR) [9, 10].

Considering the advantages of both methods, we propose a strategy that combines these two approaches instead of choosing one over the other depending on the application scenario. The proposed strategy involves switching sub-arrays over time, capitalizing on the correlation between antenna sub-arrays. This strategy aims to enhance imaging quality even further compared to using CRB or BRB criteria alone, while simultaneously reducing computational complexity compared to using the full antenna array.

The switching strategy involves dynamically selecting different sub-arrays over time, alternating between the CRB-based and the BRB-based sub-arrays. The imaging algorithm is formulated based on the expectation-maximization (EM) algorithm, which is a well-known iterative algorithm for maximum likelihood (ML) estimation [11]. The proposed strategy and imaging algorithm are validated using numerical simulations. The imaging quality is evaluated using the normalized mean square error (NMSE) and structural similarity (SSIM) metrics, both globally and locally. Results demonstrate that the proposed antenna sub-array switching strategy effectively enhances imaging quality. Moreover, the reduction in computational complexity is significant, as the number of visibilities and antennas used in the switching strategy is smaller than that of the union of the CRB-based and the BRB-based sub-arrays. This reduction in computational complexity has practical implications for real-world radio-astronomy imaging systems, allowing for more efficient data processing and reduced resource requirements.

The rest of paper is organized as follows. Section II presents the radio-interferometric data model. The antenna sub-array switching strategy is described and the corresponding EM-based imaging algorithm is formulated in Section III. Numerical setup and result analysis are presented in Section IV. Finally, Section V concludes the paper.

The following notations are used in this paper: the conjugate transpose, determinant, trace, and expectation operators are given by $(\cdot)^H$, $|\cdot|$, $\mathrm{Tr}(\cdot)$, and $\mathbb{E}[\cdot]$, respectively. The weighted ℓ_2-norm is defined as $\|\mathbf{z}\|_{\mathbf{A}}^2 = \mathbf{z}^H\mathbf{A}\mathbf{z}$ where $\mathbf{z}$ and $\mathbf{A}$ are respectively a vector and a matrix with appropriate dimensions.

II. Radio interferometric data model

The radio interferometer involves measuring the spatial coherence of the electric field between pairs of antennas in the antenna array. These measurements, known as visibilities, provide information about the electromagnetic radiation emitted by celestial sources under observation. The main idea of this paper is to dynamically switch the antenna sub-arrays

during the observation process. This can be mathematically formulated as

$$\mathbf{y}_k = \mathbf{M}_k \mathbf{r}_k,\ k = 1, \cdots, K \tag{1}$$

where $\mathbf{M}_k$ represents the switching matrix of size $p_k \times N$ (N the total number of visibilities), which is constructed by selecting $p_k < N$ rows from the identity matrix $\mathbf{I}_N$. The vector $\mathbf{r}_k$ denotes the complete visibility vector, while $\mathbf{y}_k$ represents the observed visibilities in the k-th snapshot block with K denoting the total number of snapshot blocks.

For each visibility vector $\mathbf{r}_k$, as described in [12, 13], the imaging problem in radio-astronomy can be formulated as a linear model

$$\mathbf{r}_k = \mathbf{H}\mathbf{x} + \mathbf{n}_k \tag{2}$$

where $\mathbf{H} \in \mathbb{C}^{N \times m}$ is the forward operator, which corresponds to the Fourier transform based on the Van-Cittert Zernike theorem [14], symbol $\mathbf{x} \in \mathbb{R}^m$ represents the image vector of size m (number of pixels) to be restored, and $\mathbf{n}_k \in \mathbb{C}^N$ is the noise vector corresponding to the k-th snapshot block.

The noise $\mathbf{n}_k$ can be modeled as a combination of Radio Frequency Interference (RFI) and thermal noise. RFI refers to unwanted signals or electromagnetic emissions that originate from various man-made sources, such as communication systems, satellites, power lines, or other electronic devices [15, 16]. The RFI noise can be modeled as a low rank matrix and can be removed at the stage of antenna calibration [17]. On the other hand, thermal noise is inherent to any electronic system and arises due to the random motion of electrons and thermal energy. The thermal noise is modeled as a complex Gaussian distribution with zero mean and covariance matrix $\sigma^2 \mathbf{I}_N$, where σ^2 is the thermal noise variance. For our analysis, we will first consider a general noise covariance matrix $\mathbf{\Sigma}$ for the noise vector $\mathbf{n}_k$ to account for both thermal noise and RFI. Then, we assume that the RFI noise can be removed during the antenna calibration process, and therefore, we will also give the result of the thermal noise case.

Our objective is to estimate the image vector $\mathbf{x}$ and the noise variance $\mathbf{\Sigma}$ from the noisy visibilities $\mathbf{y}_k$ with $k = 1, \cdots, K$. Furthermore, we assume that the source image $\mathbf{x}$ exhibits sparsity in the context of radio astronomy. To enforce sparsity, we incorporate an ℓ_1-norm regularization term [18] on the image vector $\mathbf{x}$

$$\mathcal{R}(\mathbf{x}) = \alpha \|\mathbf{x}\|_1 = \alpha \sum_{i=1}^{m} |x_i| \tag{3}$$

where x_i is the i-th element of $\mathbf{x}$, and α is a positive tuning parameter. A higher value of α promotes a sparser image vector $\mathbf{x}$, resulting in more elements of $\mathbf{x}$ being zero.

We will initially attempt to solve the problem using the ML estimator. The log-likelihood function of the observed visibilities is defined as

$$\begin{aligned} &L(\mathbf{y}_1, \cdots, \mathbf{y}_K | \mathbf{x}, \mathbf{\Sigma}) = \sum_{k=1}^{K} \log p(\mathbf{y}_k | \mathbf{x}, \mathbf{\Sigma}) - \alpha \|\mathbf{x}\|_1 \\ &= \sum_{k=1}^{K} \log \mathcal{CN}(\mathbf{y}_k | \mathbf{M}_k \mathbf{H}\mathbf{x}, \mathbf{M}_k \mathbf{\Sigma} \mathbf{M}_k^H) - \alpha \|\mathbf{x}\|_1 \\ &\propto - \sum_{k=1}^{K} \left(\log |\mathbf{M}_k \mathbf{\Sigma} \mathbf{M}_k^H| + \|\mathbf{e}_k\|^2_{(\mathbf{M}_k \mathbf{\Sigma} \mathbf{M}_k^H)^{-1}} \right) \\ &\quad - \alpha \|\mathbf{x}\|_1 \end{aligned} \tag{4}$$

where the symbol $\propto$ means that the irrelevant constant terms are omitted,

$$\mathbf{e}_k \triangleq \mathbf{y}_k - \mathbf{M}_k \mathbf{H}\mathbf{x} \tag{5}$$

and $\mathcal{CN}(\mathbf{y}_k | \mathbf{M}_k \mathbf{H}\mathbf{x}, \mathbf{M}_k \mathbf{\Sigma} \mathbf{M}_k^H)$ represents the probability density function of the complex Gaussian distribution with mean $\mathbf{M}_k \mathbf{H}\mathbf{x}$ and covariance matrix $\mathbf{M}_k \mathbf{\Sigma} \mathbf{M}_k^H$.

The ML estimator is obtained by maximizing the log-likelihood function

$$\hat{\mathbf{x}}, \hat{\mathbf{\Sigma}} = \arg\max_{\mathbf{x}, \mathbf{\Sigma}} L(\mathbf{y}_1, \cdots, \mathbf{y}_K | \mathbf{x}, \mathbf{\Sigma}) \tag{6}$$

Computing $\hat{\mathbf{x}}$ and $\hat{\mathbf{\Sigma}}$ presents a challenging problem, primarily due to the time-varying nature of the switching matrix. As a result, obtaining an analytical closed-form solution becomes infeasible. To tackle this challenge, we propose the utilization of the EM algorithm to solve for ML estimators.

III. EM-BASED IMAGING ALGORITHM

The EM algorithm is an iterative algorithm that alternates between the expectation (E) step and the maximization (M) step to find the maximum of the log-likelihood [11]. In our case, we consider $\mathbf{r}_k$ with $k = 1, \cdots, K$ as the complete data space and $\mathbf{y}_k = \mathbf{M}_k \mathbf{r}_k$ represents the observable part of $\mathbf{r}_k$. In addition, to denote the missing part of $\mathbf{r}_k$, we introduce a switching matrix complementary to $\mathbf{M}_k$, which is denoted by $\overline{\mathbf{M}}_k \in \mathcal{R}^{(N-p_k) \times N}$ and obtained by removing the rows of $\mathbf{M}_k$ from the identity matrix $\mathbf{I}_N$. Thus, the missing part of $\mathbf{r}_k$ can be denoted by $\overline{\mathbf{M}}_k \mathbf{r}_k$.

More specifically, in this paper, we use an extension of EM algorithm, which is the Expectation-conditional maximization either (ECME) algorithm [19]. The "either" refers to the fact that the update of $\mathbf{\Sigma}$ is conducted by maximizing the conditional expectation of the complete-data log-likelihood function, and the update of $\mathbf{x}$ is performed by maximizing directly the actual (incomplete data) log-likelihood function.

The log-likelihood function of the complete data is

$$\begin{aligned} &L_c(\mathbf{r}_1, \cdots, \mathbf{r}_K | \mathbf{x}, \mathbf{\Sigma}) = \sum_{k=1}^{K} \log p(\mathbf{r}_k | \mathbf{x}, \mathbf{\Sigma}) - \alpha \|\mathbf{x}\|_1 \\ &= \sum_{k=1}^{K} \log \mathcal{CN}(\mathbf{r}_k | \mathbf{H}\mathbf{x}, \mathbf{\Sigma}) - \alpha \|\mathbf{x}\|_1 \\ &\propto - \sum_{k=1}^{K} \left(\log |\mathbf{\Sigma}| + \mathrm{Tr}\left(\mathbf{\Sigma}^{-1} (\mathbf{r}_k - \mathbf{H}\mathbf{x})(\mathbf{r}_k - \mathbf{H}\mathbf{x})^H \right) \right) \\ &\quad - \alpha \|\mathbf{x}\|_1 \end{aligned} \tag{7}$$

For the E-step, we need to compute the expectation of complete log-likelihood function with respect to the conditional distribution of the complete data given the observed data and the current estimate of the parameters. Indeed, the only term that needs to be computed is

$$\mathbf{C}_k^{(m)} = \mathbb{E}_{\mathbf{r}_k|\mathbf{y}_k,\mathbf{x}^{(m)},\mathbf{\Sigma}^{(m)}}\left[(\mathbf{r}_k - \mathbf{H}\mathbf{x})(\mathbf{r}_k - \mathbf{H}\mathbf{x})^H\right] \tag{8}$$

where $\mathbb{E}_{\mathbf{r}_k|\mathbf{y}_k,\mathbf{x}^{(m)},\mathbf{\Sigma}^{(m)}}[\cdot]$ denotes the expectation operator with respect to the conditional distribution of $\mathbf{r}_k$ given the observed data $\mathbf{y}_k$, and the estimate of parameters at the last iteration $(\mathbf{x}^{(m)}, \mathbf{\Sigma}^{(m)})$.

To simplify the notation, we temporarily omit the iteration number (m). Using the conditional distribution of the complete data given the observed data and the current estimate of the parameters, we have (see appendix for the calculations)

$$\begin{aligned}\mathbf{C}_k &= \mathbf{\Xi}_k\mathbf{\Xi}_k^H + \overline{\mathbf{M}}_k^H\mathbf{G}_k\overline{\mathbf{M}}_k \\ \mathbf{\Xi}_k &= \mathbf{M}_k^H\mathbf{e}_k + \overline{\mathbf{M}}_k^H\boldsymbol{\mu}_k\end{aligned} \tag{9}$$

where $\boldsymbol{\mu}_k$ and $\mathbf{G}_k$ are given by

$$\begin{aligned}\boldsymbol{\mu}_k &= \overline{\mathbf{M}}_k\mathbf{\Sigma}\mathbf{M}_k^H\left(\mathbf{M}_k\mathbf{\Sigma}\mathbf{M}_k^H\right)^{-1}\mathbf{e}_k \\ \mathbf{G}_k &= \overline{\mathbf{M}}_k\mathbf{\Sigma}\overline{\mathbf{M}}_k^H - \overline{\mathbf{M}}_k\mathbf{\Sigma}\mathbf{M}_k^H\left(\mathbf{M}_k\mathbf{\Sigma}\mathbf{M}_k^H\right)^{-1}\mathbf{M}_k\mathbf{\Sigma}\overline{\mathbf{M}}_k^H\end{aligned} \tag{10}$$

Thus, the surrogate function for E-step is given by

$$Q(\mathbf{\Sigma}|\mathbf{x}^{(m)}, \mathbf{\Sigma}^{(m)}) \propto -\sum_{k=1}^{K}\left(\log|\mathbf{\Sigma}| + \mathrm{Tr}\left(\mathbf{\Sigma}^{-1}\mathbf{C}_k^{(m)}\right)\right) \tag{11}$$

Then for the M-step, we need to maximize the surrogate function $Q(\mathbf{\Sigma}|\mathbf{x}^{(m)}, \mathbf{\Sigma}^{(m)})$ with respect to $\mathbf{\Sigma}$ and the solution is given by

$$\mathbf{\Sigma}^{(m+1)} = \frac{1}{K}\sum_{k=1}^{K}\mathbf{C}_k^{(m)} \tag{12}$$

To solve for $\mathbf{x}$, we maximize directly the log-likelihood function of the observed data $\mathbf{y}_k$ given the current estimate of $\mathbf{\Sigma}^{(m)}$, which is given by

$$\hat{\mathbf{x}} = \arg\min_{\mathbf{x}}\sum_{k=1}^{K}\left(\|\mathbf{e}_k\|^2_{(\mathbf{M}_k\mathbf{\Sigma}^{(m)}\mathbf{M}_k^H)^{-1}}\right) + \alpha\|\mathbf{x}\|_1 \tag{13}$$

Specifically, we use the Iterative Soft-Thresholding Algorithm (ISTA) [20] to solve the above optimization problem and the solution is

$$\mathbf{x}^{(m+1)} = \underset{\alpha||\mathbf{x}||_1}{\mathrm{prox}}\left(\mathbf{x}^{(m)} + \frac{1}{K}\sum_{k=1}^{K}(\mathbf{M}_k\mathbf{H})^H(\mathbf{M}_k\mathbf{\Sigma}\mathbf{M}_k^H)^{-1}\mathbf{e}_k^{(m)}\right) \tag{14}$$

where $\mathbf{e}_k^{(m)} = \mathbf{y}_k - \mathbf{M}_k\mathbf{H}\mathbf{x}^{(m)}$ and the proximal operator is defined as

$$\underset{\alpha||\mathbf{x}||_1}{\mathrm{prox}}\,(\mathbf{u})_i = \mathrm{sgn}(\mathbf{u}_i)\left(|\mathbf{u}_i| - \alpha\right)_+ \tag{15}$$

with

$$\left(|\mathbf{u}_i| - \alpha\right)_+ = \max(0, |\mathbf{u}_i| - \alpha) \tag{16}$$

Algorithm 1: ECME-based antenna switching imager

Data: $\mathbf{\Sigma}^{(0)}$, $\mathbf{x}^{(0)}$
Input: $\mathbf{H}$, α, and $\mathbf{y}_k$, $k = 1, \ldots, K$
Output: Estimates of $\hat{\mathbf{x}}$ and $\hat{\mathbf{\Sigma}}$
Initialisation: $\mathbf{\Sigma}^{(m)} \leftarrow \mathbf{\Sigma}^{(0)}$, $\mathbf{x}^{(m)} \leftarrow \mathbf{x}^{(0)}$
while *stop criterion not met* **do**
  E-step: for $k = 1, \ldots, K$, compute $\boldsymbol{\mu}_k$ and $\mathbf{G}_k$ using (10), and $\mathbf{C}_k^{(m)}$ using (9)
  M-step: update $\mathbf{\Sigma}^{(m+1)}$ and $\mathbf{x}^{(m+1)}$ using (12) and (14), respectively

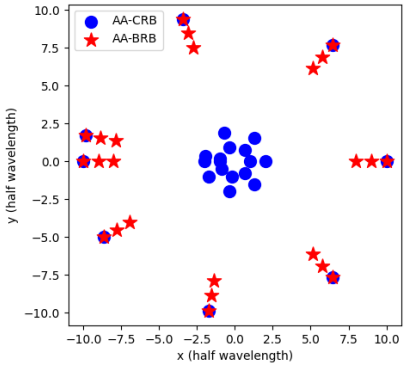

Fig. 1: Antenna configurations of the CRB-based array and the BRB-based array.

The ECME algorithm is summarized in Algorithm 1.

Remark: For the special case of considering only the thermal noise, i.e., $\mathbf{\Sigma} = \sigma^2\mathbf{I}_N$, we do not need to employ the EM algorithm, since it is possible to directly maximize the log-likelihood function in (4). In this case, the estimate of σ^2 is given by

$$\hat{\sigma}^2 = \frac{1}{\sum_{k=1}^{K} p_k}\sum_{k=1}^{K}\left\|\mathbf{e}_k^{(m)}\right\|_2^2 \tag{17}$$

and consequently, the update of $\mathbf{x}$ is given by

$$\mathbf{x}^{(m+1)} = \underset{\alpha||\mathbf{x}||_1}{\mathrm{prox}}\left(\mathbf{x}^{(m)} + \frac{1}{K\hat{\sigma}^2}\sum_{k=1}^{K}(\mathbf{M}_k\mathbf{H})^H\mathbf{e}_k^{(m)}\right) \tag{18}$$

IV. Numerical Evaluation

A. Simulation Setup

In our previous paper [21], we presented a methodology for antenna array design based on minimum error bounds. By minimizing the CRB and the BRB of the image reconstruction, we obtained the CRB-based array and the BRB-based array, respectively, as shown in Fig. 1. It is important to note that there is an intersection between the two arrays, where the correlation between the antennas is exploited by the EM algorithm to improve estimation accuracy.

In this section, we will implement the EM-based antenna switching imager using the aforementioned antenna arrays to

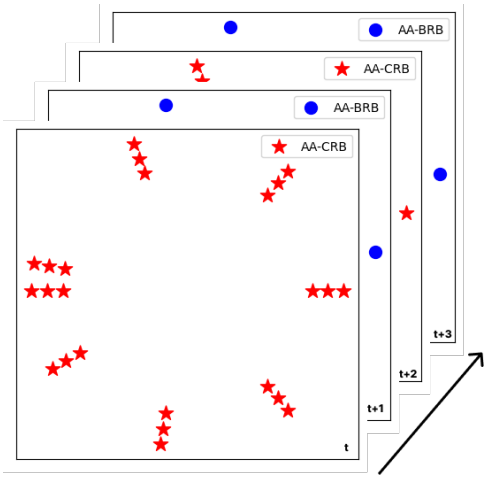

Fig. 2: Schema of the antenna switching strategy.

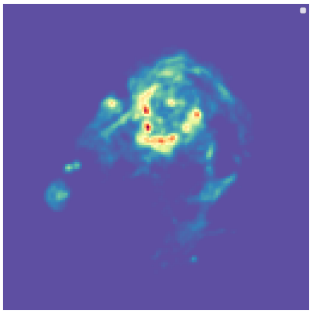

Fig. 3: True image of the M31 galaxy.

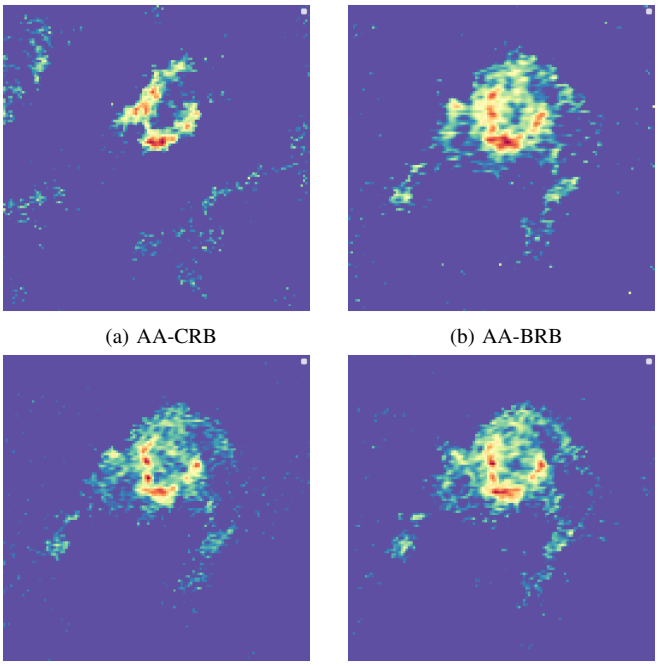

(a) AA-CRB (b) AA-BRB

(c) AA-CRB ∪ AA-BRB (d) Switching

Fig. 4: Reconstructed images of different methods. (a) AA-CRB, (b) AA-BRB, (c) AA-CRB ∪ AA-BRB, and (d) Switching.

verify the effectiveness of our proposed radio-astronomical imager. The core of the antenna array switching strategy is to alternate between the CRB-based sub-array (AA-CRB) and the BRB-based sub-array (AA-BRB). Specifically, we utilize AA-CRB at instant t, then switch to AA-BRB at instant $t+1$, and subsequently switch back to AA-CRB at instant $t+2$, and so on. The antenna switching strategy is illustrated in Fig. 2.

The specific numbers of antennas and visibilities for each method are presented in Table I. It is worth noting that the switching antenna method employs the same number of antennas as the CRB-based sub-array alone, or the BRB-based sub-array alone, which is smaller than the whole array (union of AA-CRB and AA-BRB subarrays). Additionally, the switching antenna method significantly reduces the number of visibilities compared to the whole array. Since the visibilities obtained directly from the telescope array are utilized, the switching antenna method offers a cost-effective solution for radio-astronomical imaging systems while maintaining comparable imaging performance to the full union of AA-CRB and AA-BRB.

Table I: Antenna and visibility numbers of different methods

	AA-CRB	**AA-BRB**	**Switching**	**AA-CRB∪AA-BRB**
Number of antennas	24	24	24	32
Number of visibilities	552	552	552	1616

The M31 galaxy, depicted in Fig. 3, serves as the true image for our experiments. This image is based on the H2 region in the M31 galaxy and has been previously utilized for investigating radio-astronomy imaging algorithms [22]. The M31 model image is particularly suitable for testing the effectiveness of the sparsity prior incorporated in the proposed imaging algorithms due to its ability to accurately represent both compact and extended structures.

To prepare the image for processing, the true image is discretized into $N \times N$ pixels with $N = 128$, and then vectorized, resulting in $\mathbf{x} \in \mathbb{R}^{N^2}$ in the system model. Subsequently, the true image is convolved with the point spread function (PSF) specific to each method, yielding the true visibility $\mathbf{Hx}$ for each method. In order to simulate the effects of thermal noise in the telescope arrays, additive white Gaussian noise with zero mean and a variance of σ^2 is introduced to obtain the blurred visibility. For our experiments, we set the noise variance to $\sigma^2 = 10$.

B. Performance Evaluation

The reconstructed images of different algorithms are shown in Fig. 4. It can be seen that the proposed EM-based antenna switching algorithm can reconstruct the image with almost

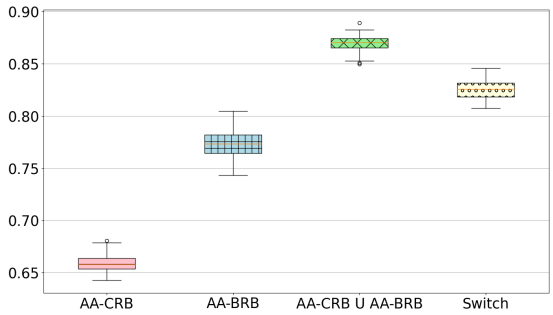

(a) SSIM

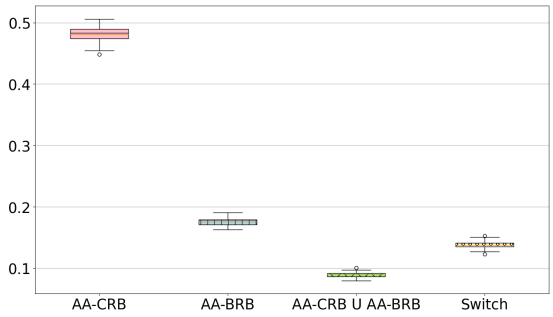

(b) NMSE

Fig. 5: Performance comparison of different methods. (a) SSIM, (b) NMSE.

the same quality as the AA-CRB∪AA-BRB, which is the union of the CRB-based sub-array and the BRB-based sub-array. The quality of the AA-CRB is the worst among all the configurations. The quality of the AA-BRB is better than the AA-CRB, but worse than the proposed EM-based antenna switching algorithm.

To better evaluate the performance of different algorithms, we perform $n_{\text{MC}} = 100$ Monte Carlo simulations, and we employ several metrics to evaluate the reconstruction error of the proposed algorithm, which are the normalized mean square error (NMSE) and the structural similarity index (SSIM). As a global metric, the NMSE is defined as

$$\text{NMSE} = \frac{\|\mathbf{x} - \hat{\mathbf{x}}\|_2^2}{\|\mathbf{x}\|_2^2} \tag{19}$$

where $\mathbf{x}$ is the true image and $\hat{\mathbf{x}}$ is the reconstructed image. The SSIM is a local metric, which is used to measure the similarity between two images [23] and is defined as

$$\text{SSIM} = \frac{(2\mu_x\mu_{\hat{x}} + c_1)(2\sigma_{x\hat{x}} + c_2)}{(\mu_x^2 + \mu_{\hat{x}}^2 + c_1)(\sigma_x^2 + \sigma_{\hat{x}}^2 + c_2)} \tag{20}$$

where μ_x and $\mu_{\hat{x}}$ are the mean values of $\mathbf{x}$ and $\hat{\mathbf{x}}$, respectively, σ_x^2 and $\sigma_{\hat{x}}^2$ are the variances of $\mathbf{x}$ and $\hat{\mathbf{x}}$, respectively, and $\sigma_{x\hat{x}}$ is the covariance of $\mathbf{x}$ and $\hat{\mathbf{x}}$. The constants c_1 and c_2 are used to stabilize the division with weak denominator. The SSIM is a value between -1 and 1, where 1 means the two images are identical.

As shown in Fig. 5, the proposed EM-based antenna switching algorithm achieves the best performance among all the 24-antenna configurations. The NMSE of the proposed algorithm is about 0.14, which is much smaller than that of AA-CRB and smaller than that of AA-BRB. The SSIM of the proposed algorithm is about 0.82, which is much larger than that of AA-CRB and also larger than that of AA-BRB. The performance of the proposed algorithm is slightly worse, but comparable with that of AA-CRB∪AA-BRB. The performance of the AA-CRB is the worst among all the configurations, but remains useful when used as part of a sub-array switching strategy. The performance of the AA-BRB is better than the AA-CRB, but worse than the proposed EM-based antenna switching algorithm.

V. Conclusions

The exploitation of the antenna sub-arrays in the radio-astronomy imaging problem is investigated in this paper. An EM-based antenna switching imaging algorithm was proposed to exploit the antenna sub-arrays. We conducted radio-astronomical imaging simulations based on the sub-arrays designed with CRB and BRB criteria. Two metrics, the NMSE and the SSIM, were adopted to evaluate the performance of different configurations. The simulation results revealed that the proposed algorithm can achieve almost the same performance as the union of the sub-arrays while reducing dramatically the number of visibilities, which means reducing the data transmission, the storage pressure, and the computational load.

Appendix

A. Conditional distribution

Given that $\mathbf{r}_k \sim \mathcal{CN}(\mathbf{Hx}, \mathbf{\Sigma})$, we can deduce

$$\begin{aligned} \mathbf{M}_k\mathbf{r}_k &\sim \mathcal{CN}(\mathbf{M}_k\mathbf{Hx}, \mathbf{M}_k\mathbf{\Sigma}\mathbf{M}_k^H) \\ \overline{\mathbf{M}}_k\mathbf{r}_k &\sim \mathcal{CN}(\overline{\mathbf{M}}_k\mathbf{Hx}, \overline{\mathbf{M}}_k\mathbf{\Sigma}\overline{\mathbf{M}}_k^H) \end{aligned} \tag{21}$$

Moreover, the covariance between $\mathbf{M}_k\mathbf{r}_k$ and $\overline{\mathbf{M}}_k\mathbf{r}_k$ is

$$\text{cov}(\mathbf{M}_k\mathbf{r}_k, \overline{\mathbf{M}}_k\mathbf{r}_k) = \mathbf{M}_k\mathbf{\Sigma}\overline{\mathbf{M}}_k^H \tag{22}$$

Thus, the joint distribution of $\mathbf{y}_k$ and $\overline{\mathbf{M}}_k\mathbf{r}_k$ is given by

$$\begin{pmatrix} \mathbf{y}_k \\ \overline{\mathbf{M}}_k\mathbf{r}_k \end{pmatrix} \sim \mathcal{CN}\left(\begin{bmatrix} \mathbf{M}_k\mathbf{Hx} \\ \overline{\mathbf{M}}_k\mathbf{Hx} \end{bmatrix}, \begin{bmatrix} \mathbf{M}_k\mathbf{\Sigma}\mathbf{M}_k^H & \mathbf{M}_k\mathbf{\Sigma}\overline{\mathbf{M}}_k^H \\ \overline{\mathbf{M}}_k\mathbf{\Sigma}\mathbf{M}_k^H & \overline{\mathbf{M}}_k\mathbf{\Sigma}\overline{\mathbf{M}}_k^H \end{bmatrix} \right) \tag{23}$$

where $\mathbf{y}_k = \mathbf{M}_k\mathbf{r}_k$.

Consequently, by defining $\boldsymbol{\mu}_k$ and $\mathbf{G}_k$ as given in (10), the conditional distribution of $\overline{\mathbf{M}}_k\mathbf{r}_k$ given $\mathbf{y}_k$ is

$$\overline{\mathbf{M}}_k\mathbf{r}_k|\mathbf{y}_k \sim \mathcal{CN}(\overline{\mathbf{M}}_k\mathbf{Hx} + \boldsymbol{\mu}_k, \mathbf{G}_k) \tag{24}$$

B. Proof of (9)

Consider the matrix $\mathbf{B}_k$ defined as

$$\mathbf{B}_k = \begin{bmatrix} \mathbf{M}_k \\ \overline{\mathbf{M}}_k \end{bmatrix} = \begin{bmatrix} \mathbf{M}_k^T & \overline{\mathbf{M}}_k^T \end{bmatrix}^T \tag{25}$$

which satisfies

$$\mathbf{B}_k^T\mathbf{B}_k = \mathbf{M}_k^T\mathbf{M}_k + \overline{\mathbf{M}}_k^T\overline{\mathbf{M}}_k = \mathbf{I}_N \tag{26}$$

and then,

$$\begin{aligned}&\mathbb{E}_{\overline{\mathbf{M}}_k\mathbf{r}_k|\mathbf{y}_k}\left[\mathbf{B}_k(\mathbf{r}_k-\mathbf{H}\mathbf{x})(\mathbf{r}_k-\mathbf{H}\mathbf{x})^H\mathbf{B}_k^T\right]\\&=\mathbb{E}_{\overline{\mathbf{M}}_k\mathbf{r}_k|\mathbf{y}_k}\begin{bmatrix}\mathbf{e}_k\mathbf{e}_k^H & \mathbf{e}_k\mathbf{r}_k^H\overline{\mathbf{M}}_k^T\\ \overline{\mathbf{M}}_k\mathbf{r}_k\mathbf{e}_k^H & \overline{\mathbf{M}}_k\mathbf{r}_k\mathbf{r}_k^H\overline{\mathbf{M}}_k^T\end{bmatrix}\end{aligned}\tag{27}$$

where $\mathbf{e}_k=\mathbf{y}_k-\mathbf{M}_k\mathbf{H}\mathbf{x}$.

Thus, after some algebra, we have

$$\begin{aligned}&\mathbb{E}_{\overline{\mathbf{M}}_k\mathbf{r}_k|\mathbf{y}_k}\left[(\mathbf{r}_k-\mathbf{H}\mathbf{x})(\mathbf{r}_k-\mathbf{H}\mathbf{x})^H\right]\\&=\mathbf{B}_k^T\mathbb{E}_{\overline{\mathbf{M}}_k\mathbf{r}_k|\mathbf{y}_k}\left[\mathbf{B}_k(\mathbf{r}_k-\mathbf{H}\mathbf{x})(\mathbf{r}_k-\mathbf{H}\mathbf{x})^H\mathbf{B}_k^T\right]\mathbf{B}_k\\&=\begin{bmatrix}\mathbf{M}_k^T & \overline{\mathbf{M}}_k^T\end{bmatrix}\begin{bmatrix}\mathbf{e}_k\mathbf{e}_k^H & \mathbf{e}_k\boldsymbol{\mu}_k^H\\ \boldsymbol{\mu}_k\mathbf{e}_k^H & \mathbf{G}_k+\boldsymbol{\mu}_k\boldsymbol{\mu}_k^H\end{bmatrix}\begin{bmatrix}\mathbf{M}_k\\ \overline{\mathbf{M}}_k\end{bmatrix}\\&=\boldsymbol{\Xi}_k\boldsymbol{\Xi}_k^H+\overline{\mathbf{M}}_k^H\mathbf{G}_k\overline{\mathbf{M}}_k\end{aligned}\tag{28}$$

resulting in $\boldsymbol{\Xi}_k$ as defined in (9).

REFERENCES

[1] C. Carilli and S. Rawlings, "Motivation, key science projects, standards and assumptions," *New Astronomy Reviews*, vol. 48, no. 11-12, pp. 979–984, 2004.

[2] P. Dewdney *et al.*, "Ska1 system baseline design v2," *SKA Organisation, Design Report SKA-TEL-SKO-0000002, Rev*, vol. 3, 2016.

[3] R. Braun, A. Bonaldi, T. Bourke, E. Keane, and J. Wagg, "Anticipated ska1 science performance," in *SKA-TEL-SKO-0000818*, 2017.

[4] F. Boone, "Interferometric array design: Distributions of fourier samples for imaging," *Astronomy & Astrophysics*, vol. 386, no. 3, pp. 1160–1171, 2002.

[5] J. P. Delmas, M. N. El Korso, H. Gazzah, and M. Castella, "CRB analysis of planar antenna arrays for optimizing near-field source localization," *Signal Processing*, vol. 127, pp. 117–134, 2016.

[6] M. N. El Korso, A. Renaux, R. Boyer, and S. Marcos, "Deterministic performance bounds on the mean square error for near field source localization," *IEEE transactions on signal processing*, vol. 61, no. 4, pp. 871–877, 2012.

[7] M. Juhlin and A. Jakobsson, "Optimal sensor placement for localizing structured signal sources," *Signal Processing*, p. 108679, 2022.

[8] J. Tabrikian, O. Isaacs, and I. Bilik, "Cognitive antenna selection for automotive radar using bobrovsky-zakai bound," *IEEE Journal of Selected Topics in Signal Processing*, vol. 15, no. 4, pp. 892–903, 2021.

[9] R. McAulay and E. Hofstetter, "Barankin bounds on parameter estimation," *IEEE Transactions on Information Theory*, vol. 17, no. 6, pp. 669–676, 1971.

[10] M. Morelande and B. Ristic, "Signal-to-noise ratio threshold effect in track before detect," *IET radar, sonar & navigation*, vol. 3, no. 6, pp. 601–608, 2009.

[11] A. P. Dempster, N. M. Laird, and D. B. Rubin, "Maximum likelihood from incomplete data via the em algorithm," *Journal of the royal statistical society: series B (methodological)*, vol. 39, no. 1, pp. 1–22, 1977.

[12] A. Dabbech, C. Ferrari, D. Mary, E. Slezak, O. Smirnov, and J. S. Kenyon, "Moresane: Model reconstruction by synthesis-analysis estimators-a sparse deconvolution algorithm for radio interferometric imaging," *Astronomy & Astrophysics*, vol. 576, p. A7, 2015.

[13] L. Pratley, J. D. McEwen, M. d'Avezac, R. E. Carrillo, A. Onose, and Y. Wiaux, "Robust sparse image reconstruction of radio interferometric observations with purify," *Monthly Notices of the Royal Astronomical Society*, vol. 473, no. 1, pp. 1038–1058, 2018.

[14] A. R. Thompson, J. M. Moran, and G. W. Swenson, *Interferometry and synthesis in radio astronomy*. Springer Nature, 2017.

[15] A.-J. Boonstra, S. J. Wijnholds, S. van der Tol, and B. Jeffs, "Calibration, sensitivity and rfi mitigation requirements for lofar," in *Proceedings.(ICASSP'05). IEEE International Conference on Acoustics, Speech, and Signal Processing, 2005.*, vol. 5. IEEE, 2005, pp. v–869.

[16] W. A. Baan, "Implementing rfi mitigation in radio science," *Journal of Astronomical Instrumentation*, vol. 8, no. 01, p. 1940010, 2019.

[17] Y. Mhiri, M. N. El Korso, A. Breloy, and P. Larzabal, "Multifrequency array calibration in presence of radio frequency interferences," *Signal Processing*, vol. 199, p. 108613, 2022.

[18] Y. Mhiri, M. N. El Korso, A. Breloy, and P. Larzabal, "A robust em algorithm for radio interferometric imaging in the presence of outliers," in *2022 IEEE Workshop on Signal Processing Systems (SiPS)*. IEEE, 2022, pp. 1–5.

[19] C. Liu and D. B. Rubin, "The ecme algorithm: a simple extension of em and ecm with faster monotone convergence," *Biometrika*, vol. 81, no. 4, pp. 633–648, 1994.

[20] A. Beck and M. Teboulle, "A fast iterative shrinkage-thresholding algorithm for linear inverse problems," *SIAM journal on imaging sciences*, vol. 2, no. 1, pp. 183–202, 2009.

[21] J. Wang, L. Bacharach, M. N. El Korso, and P. Larzabal, "Barankin bound vs Cramér-Rao bound for interferometric-like array design at low SNR," in *2023 31st European Signal Processing Conference (EUSIPCO)*. IEEE, 2023, pp. 1–5, accpeted.

[22] R. E. Carrillo, J. D. McEwen, and Y. Wiaux, "Purify: a new approach to radio-interferometric imaging," *Monthly Notices of the Royal Astronomical Society*, vol. 439, no. 4, pp. 3591–3604, 2014.

[23] R. Dosselmann and X. D. Yang, "A comprehensive assessment of the structural similarity index," *Signal, Image and Video Processing*, vol. 5, pp. 81–91, 2011.